


RESEARCH ARTICLE OPEN ACCESS

Beta-Lactam Antibiotics Promote Extracellular Vesicle Production of *Staphylococcus aureus* Through ROS-Mediated Lipid Metabolic Reprogramming

Xiaonan Huang¹ | Zhen Hu¹ | Weilong Shang¹ | Juan Chen² | Qiwen Hu¹ | Yumin Zhou³ | Ruolan Ding⁴ | Jing Yin⁵ | Mengyang Li⁴ | He Liu¹ | Jianxiong Dou¹ | Huagang Peng¹ | Yifan Rao⁶ | Lu Liu¹ | Yuting Wang¹ | Li Tan¹ | Yuhua Yang¹ | Jianghong Wu^{1,6} | Chuan Xiao¹ | Yi Yang¹ | Xiancai Rao^{1,4} 

¹Department of Microbiology, College of Basic Medical Sciences, Key Laboratory of Microbial Engineering under the Educational Committee in Chongqing, Army Medical University, Chongqing, China | ²Department of Pharmacy, Xinqiao Hospital, Army Medical University, Chongqing, China | ³Department of Dermatology, Southwest Hospital, Army Medical University, Chongqing, China | ⁴Department of Microbiology, School of Medicine, Chongqing University, Chongqing, China | ⁵Department of Neurology, First Affiliated Hospital of Kunming Medical University, Kunming, China | ⁶Department of Emergency Medicine, Xinqiao Hospital, Army Medical University, Chongqing, China

Correspondence: Yi Yang (yangyi980783@tmmu.edu.cn) | Xiancai Rao (raoxiancai@126.com)

Received: 21 November 2024 | **Accepted:** 26 March 2025

Funding: This work was supported by the National Natural Science Foundation of China (No. 82071857).

Keywords: β -lactam antibiotics | extracellular vesicle | lipid metabolism | penicillin binding proteins | reactive oxygen species | *Staphylococcus aureus*

ABSTRACT

Bacterial extracellular vesicles (EVs) are natural reservoirs of biological active substances. They exhibit promising application in developing bioproducts such as vaccine, drug-delivery system and anticancer agent. However, the low yield of naturally secreted EVs during bacterial growth is a bottleneck factor that restricts EV applications. In this study, we showed that sub-minimum inhibitory concentration (MIC) of β -lactams boosted EV production in various *Staphylococcus aureus* strains. The expression of penicillin-binding protein (PBP) genes increased after β -lactam treatment, and the inactivation of alternative PBPs promoted EV secretion of *S. aureus*. We also demonstrated that sub-MIC β -lactams promoted EV production via a reactive oxygen species (ROS)-dependent pathway. Deletion of redundant *pbp* genes enhanced oxacillin (OXA)-stimulated ROS levels. Transcriptomic and lipidomic analyses revealed that OXA-induced ROS triggered lipid metabolic reprogramming in *S. aureus*. Particularly, ROS promoted lipid peroxidation (LPO) and increased the biosynthesis of phosphatidic acid (PA) and lipoteichoic acid (LTA) that contributed to EV generation. Furthermore, OXA treatment altered the diversity of EV-loaded proteins. OXA-treated Δ_{agr}/OXA EVs induced stronger Dengue EDIII-specific antibodies in BALB/c mice than did Δ_{agr} EVs. Overall, this study provided mechanistic insights into β -lactam-promoted EV production in *S. aureus*, and highlighted the potential strategies to prepare EVs for various applications.

Xiaonan Huang and Zhen Hu contributed equally to this work.

This is an open access article under the terms of the [Creative Commons Attribution-NonCommercial](https://creativecommons.org/licenses/by-nc/4.0/) License, which permits use, distribution and reproduction in any medium, provided the original work is properly cited and is not used for commercial purposes.

© 2025 The Author(s). *Journal of Extracellular Vesicles* published by Wiley Periodicals LLC on behalf of International Society for Extracellular Vesicles.

1 | Introduction

The secretion of spherical nanostructures is a common process across all life forms. The extracellular vesicles (EVs) produced by bacteria are nanosized bilayer particles (Toyofuku et al. 2023). Benefiting from their rich cargos such as proteins, nucleic acids, lipids, polysaccharides and many other bioactive substances (Kim et al. 2015; Bitto et al. 2021a), bacterial EVs play vital roles in various biological processes, including horizontal gene transfer (Domingues and Nielsen 2017), biofilm formation (Jeong et al. 2024) and host–microbe communication (Kaparakis-Liaskos and Ferrero 2015). Notably, with the development of genetic engineering technologies, the application of bacterial EVs in developing new concepts of biological products is attracting considerable attention (Qiao et al. 2021). Bacterial EVs can serve as vaccines. The successful EV vaccine MenB-4C has been approved to prevent invasive meningococcal disease (Abitbol et al. 2024). Moreover, EVs can serve as delivery platforms for various bioagents, such as drugs (Collins and Brown 2021), nucleic acids (Li et al. 2022) and exogenous antigens (Hu et al. 2022). In a previous study, we engineered an accessory gene regulator (*agr*) deletion mutant RN4220 Δ *agr*/EDIII carrying degenerate EDIII antigens (EDIII_{conA} and EDIII_{conB}) of Dengue virus serotype 1–4 (DENV1–4), and its EVs can successfully induce protective immune responses against a lethal dose of DENV-2 infection in mice (Yuan et al. 2018). Bacterial EVs have also been proven to exhibit unique antitumor efficiency through activating host immune response or causing programmed tumour-cell death (Kim et al. 2017; Li et al. 2024). Thus, bacterial EV-originated products demonstrate encouraging application prospects in the field of life sciences (Huang et al. 2022; Suri et al. 2023). However, the yields of naturally released EVs from bacteria under normal growth conditions are extremely low, thereby severely hampering EV potential applications. Boosting EV production in certain bacteria is an urgent problem to be solved.

The process of bacterial EV formation and secretion has been preliminarily investigated. A typical process may include EV budding from bacterial cell membrane, shedding and forming round membranous structures, and secreting into external environment through the cell wall (Toyofuku et al. 2018). Variations in bacterial structures, such as membrane instability and curvature (Wang et al. 2018; McMillan and Kuehn 2021), as well as peptidoglycan cross-linking degree (Wang et al. 2018), considerably affect EV secretion. Particularly, the thick and compact cell walls of Gram-positive bacteria pose a major impediment to EV release. Theoretically, weakening the bacterial cell wall structure can effectively promote EV production. Toyofuku et al. (2017) reported that prophage-encoded endolysin can generate holes in cell wall to enhance EV release from *Bacillus subtilis*. The introduction of an autonomous controlled peptidoglycan hydrolase (PGase) expression system elevates the EV yields in both Gram-positive and Gram-negative bacteria (Liu et al. 2023). β -Lactams are powerful antibiotics that interfere with bacterial cell wall synthesis, and evidences prove that β -lactams at low concentrations can promote EV production (Wang et al. 2018; Kim et al. 2020). However, the mechanisms underlying β -lactam-stimulated EV release remain unclear. Several studies have demonstrated the alterations in bacterial growth rate, gene expression and metabolic state under antibiotic stress (Hu et al. 2016; Hodille et al. 2017; Chen et al. 2021). The impacts of these

changes on the components and biological functions of bacterial EVs need to be elucidated.

In the present study, the universal promotion effects of sub-minimum inhibitory concentrations (MICs) of β -lactam antibiotics on EV generation were demonstrated in Gram-positive *Staphylococcus aureus* with diverse genetic lineages. Antibiotic exposure increased bacterial reactive oxygen species (ROS) generation in *S. aureus* strains (RN4220 and RN4220 Δ *agr*/EDIII) and induced EV secretion in a ROS-dependent manner. The penicillin-binding proteins (PBPs) that bind directly to β -lactams limited the production of ROS and EVs in *S. aureus* under oxacillin (OXA) stress, whilst the inactivation of alternative PBPs improved OXA-induced EV secretion. OXA-induced ROS promoted EV formation mainly by reprogramming bacterial lipid metabolism, particularly, increasing the biosynthesis of phosphatidic acid (PA) and lipoteichoic acid (LTA). Moreover, OXA treatment changed EV protein contents and its immunogenicity. Notably, OXA-induced EVs (Δ *agr*/OXA EVs) derived from RN4220 Δ *agr*/EDIII stimulated stronger levels of DENV-specific IgG, IgG1 and IgG2a antibodies than untreated Δ *agr* EVs with equal protein contents. Overall, our study uncovers a mechanism underlying β -lactam-induced EV production in *S. aureus*. β -Lactam treatment and PBP inactivation are promising strategies to prepare EVs for applications.

2 | Materials and Methods

2.1 | Bacterial Strains, Plasmids and Primers

Bacterial strains and plasmids used in this study are listed in Table S1. *S. aureus* strains were cultured in brain heart infusion (BHI) broth (Oxoid, UK) at 37°C with shaking at 200 rpm. *Escherichia coli* strains were grown in Luria-Bertani (LB) broth (Oxoid, UK). All primers used are listed in Table S2.

2.2 | Isolation and Quantification of Bacterial EVs

Bacterial EVs were isolated from the culture supernatants as previously described with some modifications (Wang et al. 2018; Wang et al. 2025). Briefly, *S. aureus* strains were cultured overnight in BHI medium supplemented with appropriate antibiotics at 37°C with shaking. Then, bacterial culture was centrifuged at 6000 \times g for 10 min at 4°C, and culture supernatants were filtered through a 0.22 μ m filter (Merck Millipore, USA). Next, the filtrate was concentrated by a 100 kDa hollow fibre membrane column (GE Healthcare, USA), and centrifuged at 200,000 \times g for 3 h at 4°C (HITACHI, Japan) using a P70AT rotor. The EV pellets were washed once with PBS, and resuspended in PBS. The primary EV samples were loaded to the density gradient solution prepared with 4 mL of 50% Optiprep (Alere Technologies AS, Norway), 2 mL of 40% Optiprep, 2 mL of 20% Optiprep and 1.5 mL of 10% Optiprep. After horizontal centrifugation at 200,000 \times g for 3 h at 4°C using a P40ST rotor, the solution was divided into six fractions from top to bottom which were transferred into six sterilised Eppendorf tubes, respectively. Each fraction was visualised by silver-stained sodium dodecyl sulphate polyacrylamide gel electrophoresis (SDS-PAGE; Servicebio, China) and examined by transmission electron microscopy (TEM), to identify

which fraction contained the purified EVs. Finally, the purified EV samples located between second and fourth fractions were concentrated using ultrafiltration tube (Millipore, Germany), and kept at -80°C .

To avoid bacterial contamination during EV preparation, all tubes and glass containers were sterilised, and the reagents dissolved in sterilised PBS were filtered with the $0.22\text{ }\mu\text{m}$ filters. The collected EV samples were dissolved in sterilised PBS, and $10\text{ }\mu\text{L}$ of the samples were dropped onto BHI agar plates for bacterial counting after culture at 37°C overnight.

2.3 | Quantitative Analysis and Characterisation of EVs

The protein profiles of EV samples were analysed by SDS-PAGE. Briefly, protein bands of equal volumes of primary EV samples were separated by 12% (w/v) SDS-PAGE, stained with Coomassie brilliant blue and photographed. The protein concentrations of primary EVs were detected using a Bradford protein assay kit (Beyotime, China). For detection of lipid concentration, $5\text{ }\mu\text{L}$ of primary EVs were stained with FM4-64 lipid dye ($200\text{ }\mu\text{L}$ at a concentration of $5\text{ }\mu\text{g/mL}$; Coolaber, China) for 10 min at 37°C , and the fluorescence intensity of samples was determined with 515 nm excitation and 640 nm emission as previously described (Briaud et al. 2021; Rao et al. 2022). The particle number and size of EVs were analysed using resistive pulse sensing (RPS) via Nanocoulter G (Resun Technology, China). A nanometre pore chip with a measurement range of 50–250 nm was used. All EV samples were diluted with PBS to the concentrations of about 7×10^8 to 5×10^{10} particles per millilitre; the samples prepared from BHI media were used as blank controls. The final particle number of EV samples was determined by subtracting the particle numbers of blank controls from EV samples. The protein and lipid concentrations, as well as the particle numbers of EVs, were normalised with the volume of the culture medium.

2.4 | Detection of Antibiotic Susceptibility

The MICs of antibiotics against different *S. aureus* strains were determined by the broth dilution method. Briefly, bacterial cells were adjusted to a concentration of 1×10^6 CFU/mL with Mueller-Hinton broth (MHB, Solarbio, China). The bacterial solutions were added to 24-well plates (1 mL/well ; Corning, USA). The vancomycin (VAN, $16\text{ }\mu\text{g/mL}$), erythromycin (ERY, $0.5\text{ }\mu\text{g/mL}$), OXA ($4\text{ }\mu\text{g/mL}$), imipenem (IMP, $0.5\text{ }\mu\text{g/mL}$) and cefotaxime (CTX, $8\text{ }\mu\text{g/mL}$) were two-fold diluted with MHB for six times. Cefoxitin (FOX) and chloramphenicol (CAP) were adjusted to the concentrations of 10, 8, 6, 4, 2 and 1 mg/L . Kanamycin (KAN) was adjusted to 28, 24, 20, 16, 12 and $8\text{ }\mu\text{g/mL}$. Cefaclor (CEC) was adjusted to 25, 20, 15, 10, 5 and $2.5\text{ }\mu\text{g/mL}$. Then, 1 mL of each diluted antibiotic solution was added and mixed with bacterial solutions. The plates were cultured at 37°C for 24 h. The MICs of antibiotics were determined by the minimum drug concentration for inhibiting the visible growth of bacteria. All experiments were conducted in three biological times.

2.5 | Bacterial Growth Curve

The growth curves of *S. aureus* strains under different conditions were determined using a Spark Multimode Microplate Reader (TECAN, Austria). Briefly, overnight cultured *S. aureus* strains were 1:100 diluted in BHI medium. Reagents, including diverse antibiotics, antagonists and exogenous lipids, were added when needed. Then, $200\text{ }\mu\text{L}$ of each sample was added into a 96-well flat microplate (Corning, USA). The optical density values at 600 nm (OD_{600}) were determined every hour for 12 h after inoculation. The growth curves of bacteria were drawn using the OD_{600} values over culture times.

2.6 | RT-qPCR

Real-time quantitative reverse transcription polymerase chain reaction (RT-qPCR) was performed to detect the expression levels of *pbp* genes in RN4220 Δ agr/EDIII and lipid-synthesis-related genes in the RN4220 strain, as previously described (Rao et al. 2022). In brief, overnight cultured *S. aureus* was 1:100 diluted in BHI supplemented with or without OXA and cultured for another 4 h (2 h for lipid synthetic gene when detection). Bacterial cells were collected and resuspended in RNase-free ddH₂O and broken with zirconia particles (0.1 mm in diameter) for 100 s. After temporary centrifugation, the total RNA in the supernatant was extracted using an RNAPrep Pure Cell/Bacteria Kit (TianGen, China). The genomic DNA was removed from samples using RQ1 RNase-free DNase (Promega, USA). Then, cDNA was obtained using a RevertAid First Strand cDNA Synthesis Kit (Thermo Fisher Scientific, USA). The expression levels of the target genes were detected, and the 16S rRNA gene was used as a reference for normalisation. The relative expression level of each gene in the control group was set to 1.0. The primers used for RT-qPCR are listed in Table S2.

2.7 | Construction of *pbp3* and *pbp4* Gene Mutant Strains

The deletion of *pbp3* and *pbp4* genes in *S. aureus* RN4220 Δ agr/EDIII was performed as previously described (Yang et al. 2020). Briefly, the upstream and downstream DNA segments across the *pbp3* gene were amplified by PCR with primers *pbp3*-up-1/2 and *pbp3*-down-1/2, and cloned into a temperature-sensitive plasmid pYT3 using a homologous recombination strategy to achieve pYT3- Δ *pbp3* plasmid, which was then transformed into RN4220 Δ agr/EDIII and cultured at 30°C overnight. The plasmid-carried strain RN4220 Δ agr/EDIII was cultured at 42°C to accomplish recombination and then cultured at 25°C to promote plasmid cleavage to achieve *pbp3* gene deletion. The correct mutant was confirmed by PCR and DNA sequencing and designated as RN4220 Δ agr Δ *pbp3*/EDIII. A similar strategy was performed to obtain mutant strains RN4220 Δ agr Δ *pbp4*/EDIII and RN4220 Δ agr Δ *pbp3* Δ *pbp4*/EDIII.

2.8 | TEM Observation

An overnight culture of *S. aureus* strains was inoculated into fresh BHI medium (1:100) and cultured at 37°C for 8 h. Bacterial sam-

ples were prepared as previously reported (Yang et al. 2020) and observed under a TEM (Philips, The Netherlands). The purified EVs were dropped on the copper grids and negatively stained with 2% phosphotungstic acid for 15 s after a sedimentation of 15 min. Afterwards, the copper grids were left to dry naturally over 1 h at least and observed under TEM.

2.9 | RNA Sequencing and Analysis

Overnight cultured *S. aureus* RN4220 was inoculated into fresh BHI broth at a dilution of 1:100 and cultured at 37°C for 2 h with or without 1/2 MIC of OXA treatment. Bacterial cells were harvested, and the total RNA was isolated using the Trizol Reagent (Invitrogen Life Technologies). A Zymo-Seq RiboFree Total RNA Library Kit was used to remove rRNA from the total RNA sample. cDNA libraries were built using a Next Ultra RNA Library Prep Kit (New England Biolabs, USA). RNA sequencing (RNA-seq) was performed on the NovaSeq 6000 platform (Illumina) at Shanghai Bioprofile Technology Company Ltd.

The reference genome and gene annotation files were downloaded from the genome website (https://www.ncbi.nlm.nih.gov/datasets/genome/GCF_000212435.1/). The index of reference genome was built by Bowtie2 software version 2.5.1, and the gene read count value was counted using HTSeq (v0.9.1) as the original expression level of the gene. FPKM (fragments per kilobase of exon per million fragments mapped) was used to normalise the expression. DESeq (v1.38.3) was conducted to analyse the differentially expressed mRNA; transcripts with foldchange (FC) > 1.2 or < 0.83 and $p < 0.05$ were considered as differentially expressed mRNA. A volcano map of differentially expressed mRNAs was generated using the R language ggplot2 software package. ClusterProfiler (v4.6.0) software was used to carry out the enrichment analysis of the Kyoto Encyclopaedia of Genes and Genomes (KEGG) pathway of differential genes. KEGG enrichment analyses were performed with the Fisher's exact test, and FDR correction for multiple testing was also conducted. Enriched KEGG pathways were statistically significant at the $p < 0.05$ level. The gene set enrichment analysis (GSEA, v4.1.0) tool was used for GSEA enrichment of all genes, and a GSEA enrichment analysis pathway map was drawn.

The RNA-seq data were submitted to the sequence read archive (SRA) database with an accession number of PRJNA1174898.

2.10 | Flow Cytometry

The levels of intracellular ROS and lipid peroxidation (LPO) in *S. aureus* were detected by flow cytometry. Briefly, overnight cultured *S. aureus* strain RN4220 and its derivatives were 1:100 diluted with BHI, and sub-MICs of OXA were added when required. The ROS antagonists, including ROS scavenger ascorbic acid (ASA; Sigma, USA) at 10 mM and inhibitor 4,4'-Dimethyl-2,2'-bipyridine (DP; MedChemExpress, USA) at 0.25 mM, were added together with OXA when needed. Hydrogen peroxide (H₂O₂, 0.3%) was used as a positive control. Bacterial cells were cultured at 37°C with shaking at 200 rpm and centrifuged at 6000 × g for 5 min. Cell pellets were resuspended and adjusted to a concentration of 1 × 10⁶ CFU/mL. Approximately 500 µL

bacterial solutions were incubated with 10 µM of H2DCFDA (MedChemExpress, USA) or 5 µM of BODIPY 581/591 C11 (Sigma, USA) at 37°C for 45 min in the dark. After that, 200 µL of bacterial samples were measured via flow cytometry (Challenbio, China). The data were analysed with software Flowjo v10.8.1.

2.11 | 4D Label-Free Proteomic Analysis

Protein contents in the purified EV samples from RN4220Δ*agr*/EDIII (Δ*agr*EVs), OXA-treated RN4220Δ*agr*/EDIII (Δ*agr*/OXA EVs) and RN4220Δ*agr*Δ*pbp3*Δ*pbp4*/EDIII (Δ*agr*Δ*pbp3*Δ*pbp4*EVs) were detected by 4D-label-free liquid chromatography–tandem mass spectrometry (LC–MS/MS) as previously described (Chen et al. 2023). Bacterial samples were boiled and followed by ultrasonication. Undissolved bacterial debris was removed by centrifugation at 16,000 × g for 15 min. The supernatant was quantified with a BCA Protein Assay Kit (Bio-Rad, USA). 4D-label-free LC–MS/MS was conducted at Shanghai Bioprofile Technology Co., Ltd. (China). For MS data acquisition, the timsTOF Pro2 (Bruker) was operated in PASEF mode. The full scans were recorded from 100 to 1700 m/z spanning from 0.6 to 1.6 Vs/cm² in the mobility (1/K0) dimension. CID collision energy was set at 42 eV. The MS results were analysed for data interpretation and protein identification against the *S. aureus* [1280]-94067-20230711.fasta database from Uniprot (including 94067 protein sequences), which was sourced from the protein database at <https://www.uniprot.org/> 1280. The MS spectra were searched using MSFragger version 2.4 and FragPipe version 13.1 with mass calibration and parameter optimisation enabled. Label-free quantification analysis was performed with IonQuant (version 1.1.0). Expression data were grouped together by hierarchical clustering according to the protein or site level. The threshold for differential protein expression was a FC > 2 or < 0.5 and $p < 0.05$ when Δ*agr*Δ*pbp3*Δ*pbp4*EVs or Δ*agr*/OXA EVs compared with Δ*agr*EVs. To annotate the sequences, information was extracted from UniProtKB/Swiss-Prot and subjected to KEGG analysis.

The mass spectrometry proteomic data have been deposited to the ProteomeXchange data set (accession number PXD057038).

2.12 | Untargeted Lipidomics

S. aureus RN4220 was cultivated in BHI broth with or without 1/2 MIC of OXA for 2 h at 37°C. Bacterial cells were collected, resuspended in 400 µL of ice-cold 75% methanol and sonicated for 15 min. Then, 1 mL of tert-butyl methyl ether (Merck, German) was added to induce phase separation and acquire lipids and lipophilic metabolites. Lipid analysis was performed using Q Exactive Plus Orbitrap mass spectrometer (Thermo Fisher) coupled with UHPLC system Nexera X2 LC-30AD (Shimadzu, Japan). Samples were separated using a Hypersil GOLD C18 column (Thermo Fisher). Mobile phase A was 60% acetonitrile with 10 mM ammonium acetate. The flow rate was set to 0.3 mL/min. The gradient was 30% mobile phase B (10% acetonitrile in isopropanol) for 0.5 min, then linearly increased to 100% phase B in 10.5 min and maintained at 100% phase B for 2 min. Subsequently, the mobile solution was changed to 30% phase B in 0.1 min and maintained for 4.5 min to equilibrate

the column. The electrospray ionisation positive and negative modes were applied for MS data acquisition. The positive mode of spray voltage was 3.8 kV and the negative mode was 3.5 kV. MS data were acquired using a data-dependent Top10 method, dynamically choosing the most abundant precursor ions from the survey scan (200–1500 m/z) for high-energy collision dissociation fragmentation. Stepped normalised collision energy was set as 25, 30 or 35. Lipids were identified and quantified using MS-DIAL LipidBlast (version 68). Mass tolerance of 10 and 20 ppm was applied for precursor and product ions. A retention time shift of 0.2 min was performed in “alignment.”

SIMCAP software (Version 14.0; Umetrics, Umeå, Sweden) was used for all multivariate data analysis and modelling. The discriminating metabolites were obtained using a statistically significant threshold of variable influence on projection (VIP) values obtained from the OPLS-DA model and two-tailed Student's *t*-test (*p* value) on the normalised raw data at univariate analysis level. Metabolites with VIP values greater than 1.0 and *p* value less than 0.05 were considered as statistically significant metabolites.

2.13 | Detection of LPO and ROS Levels in EV Samples

Approximately 50 µL purified EV samples were added into 96-well flat clear-bottom black microplates (Corning, USA), and PBS was used as a blank control. A total of 150 µL of BODIPY 581/591 C11 (Sigma, USA) at a final concentration of 5 µM or 10 µM of H2DCFDA was added to detect LPO and ROS levels in EV samples. After incubating at 37°C for 45 min in the dark, the fluorescence intensity of each sample (RFU) was measured using a multimode reader (SpectraMax M2e, MolecularDevices, USA) with Ex/Em 488/525 nm. The level of LPO or ROS in the EV samples was calculated with a formula: Total LPO or ROS = ((sample [RFU] – blank control [RFU]) / 50 µL) × bulk volume of sample.

2.14 | Effect of Exogenous Lipid or Inhibitor on EV Production

To determine the effect of exogenous lipids on EV production, PA (P9511; Sigma Aldrich, USA) was dissolved in a solution (dimethylsulfoxide: ethyl alcohol : ddH₂O = 1: 2: 2) and adjusted to a concentration of 4 mg/mL. Cardiolipin (CL, C0563; Sigma) was dissolved in ethyl alcohol to a concentration of 2.5 mg/mL. Various concentrations of PA (0.04, 0.4 and 4 µg/mL) and CL (0.5, 2.5 and 10 µg/mL) were added to BHI media, which were then subjected to *S. aureus* culture. As for the LtaS inhibition experiment, 1650-M15 inhibitor (MedChemExpress, USA) was dissolved in dimethylsulfoxide to a concentration of 10 mM, and a final concentration of 10 µM was used. After treatment, the primary EV samples were prepared and quantitatively analysed by Bradford determination of protein concentrations.

2.15 | Western Blot

Dengue EDIII protein expression levels in the purified EV samples of interest were detected by Western blot. Briefly, the

purified EV proteins were separated by 12% (w/v) SDS-PAGE, transferred to a polyvinylidene fluoride (PVDF) membrane. Mouse anti-EDIII antibody (DENV-2; Sino Biological, China) in 1:5000 dilution was used as the first antibody. Goat anti-mouse IgG conjugated with horseradish peroxidase (HRP) was used as the secondary antibody. Target proteins were visualised by the enhanced chemiluminescence system (Amersham Pharmacia Biotech, USA) and photographed.

2.16 | Animal Assay

Female BALB/c mice of 6–8 weeks old were purchased from Byrness Weil biotech Ltd (China). Mice were randomly divided into four groups. At day 0, mice were intraperitoneally injected with 30 µg purified Δ_{agr} EVs, $\Delta_{agr}\Delta_{pbp3}\Delta_{pbp4}$ EVs or Δ_{agr}/OXA EVs dissolved in 100 µL PBS. Mice injected with 100 µL PBS were used as negative controls. Immunised mice were then boosted with 50 µg of the corresponding EVs at Day 10, Day 20 and Day 30, and sacrificed at Day 51. During the experiment, mouse body weights were measured every day. Serum samples were collected by tail vein bleeding before the primary immunisation, 6 h after primary immunisation, and at the endpoint time. The animal experiments were approved by the Laboratory Animal Welfare and Ethics Committee of the Army Medical University (Third Military Medical University) with a reference number of AMUWEC2020735.

2.17 | ELISA

The levels of interleukin 6 (IL-6) and tumour necrosis factor (TNF)-α in mouse sera 6 h after primary immunisation were measured using an enzyme-linked immunosorbent assay (ELISA) kit (Bioss, China) according to the product instructions. To detect the titres of Dengue EDIII-specific IgG, IgG1 and IgG2a, commercially purchased EDIII proteins (Sino Biological, China) were diluted with ELISA coating solution (0.05 M carbonate buffer, pH 9.6) and added to ELISA plates at 50 ng/well. Plates were coated at 4°C overnight, washed with PBST (PBS with 0.05% Tween-20) for three times and blocked with 5% (w/v) bovine serum albumin (BSA) at 37°C for 2 h. Then, 50 µL of serial 10-fold diluted serum samples were added into plates. After 2 h of incubation at 37°C and washing thrice with PBST, plate wells were added with 1:5000 diluted HRP-conjugated goat anti-mice IgG, IgG1 and IgG2a, respectively (Abcam, UK), and kept at 37°C for 1 h. After washing thrice with PBST, colorimetric analysis was performed using two-components tetramethylbenzidine (TMB) substrate solution (Solarbio, China) and stop solution (Solarbio, China). The OD₄₅₀ values were detected using a Bio-Tek microplate reader (Bio-Rad). The maximum dilution of serum being significantly different with the PBS group was read as the antibody titre.

2.18 | Statistics Analysis

Data analysis was performed using GraphPad Prism 10.1.2 software. Unpaired two-tailed Student's *t*-test was used to compare samples between two groups, and one-way analysis of variance (ANOVA) was used to test multiple groups. Results are presented

as the mean \pm standard deviation (SD), and a p value less than 0.05 was considered statistically significant.

3 | RESULTS

3.1 | β -Lactam Antibiotics Promoted EV Production in *S. aureus* With Various Genetic Backgrounds

To detect the effect of antibiotics on *S. aureus* EV secretion, the MICs of various antibiotics against *S. aureus* RN4220 (a methicillin-susceptible *S. aureus*, MSSA, ST8) were determined (Table S3). Then, RN4220 was cultured in BHI medium supplemented with 1/4 MIC of VAN, ERY, CAP, KAN or OXA for 12 h. The EVs were prepared from culture supernatants, and SDS-PAGE analysis revealed that only β -lactam antibiotic OXA substantially enhanced EV production (Figure 1a). The protein concentration of EVs derived from OXA-induced *S. aureus* RN4220 increased by 58-fold compared with that of EVs without antibiotic treatment (control) and 29–45 times relative to that of EVs from RN4220 treated with other tested antibiotics (Figure 1b). The EV lipid concentration after OXA treatment was 104–217-fold higher than that of the control and other antibiotic treatment groups (Figure 1c). OXA exposure increased EV particle number by 37.8–109.5 times compared with other groups (Figure 1d). Moreover, sub-MIC of OXA promoted EV secretion of *S. aureus* in a dose-dependent manner with an exception of 1/2 MIC OXA, which resulted in lower EV yield than 1/8 and 1/4 MICs (Figure 1e–h), partially due to the serious arrest of bacterial growth under 1/2 MIC OXA (Figure S1).

Subsequently, EV productions in other *S. aureus* strains treated with OXA were determined, including MSSA strain ATCC 25923 (ST243), methicillin-resistant *S. aureus* (MRSA) strain USA300 (ST8) and the vancomycin-intermediate *S. aureus* (VISA, ST239) isolate XN108 (Table S1). As shown in Figure 1i–l, all tested *S. aureus* strains considerably increased their EV production after 1/4 MIC of OXA treatment. Overall, these findings indicated that sub-MIC of β -lactam antibiotic OXA but not VAN, CAP, ERY or KAN considerably enhanced EV production in *S. aureus* with different genetic lineages.

3.2 | Inactivation of Alternative PBPs Increased EV Production in *S. aureus*

β -Lactam antibiotics primarily act on PBPs to interfere with peptidoglycan biosynthesis (Lade and Kim 2023). *S. aureus* strains encode four PBPs (PBP1–4) (Lade and Kim 2023). RT-qPCR detection showed that 1/4 MIC of OXA remarkably enhanced the expression levels of all four *pbp* genes in the strain RN4220 Δ agr/EDIII (Figure 2a), perhaps a feedback effect to the inhibition of OXA on PBP functions. OXA can bind to all four PBP molecules of *S. aureus*, we next used 1/4 MIC (Table S3) of IMP, CTX, CEC and FOX, which have priority to target PBP1, PBP2, PBP3 and PBP4, respectively (Hodille et al. 2017), to treat RN4220 Δ agr/EDIII. The results demonstrated that all tested antibiotics considerably increased EV production (Figure 2b,c), thereby confirming that β -lactams can promote EV release in *S. aureus*.

In *S. aureus*, *pbp1* and *pbp2* are essential genes (Hodille et al. 2017). We next deleted the alternative *pbp3* and *pbp4* genes in *S. aureus* RN4220 Δ agr/EDIII to mimic the inhibitory effect of β -lactam on PBP functions (Figure S2). Bacterial growths of all mutants, including RN4220 Δ agr Δ pbp3/EDIII, RN4220 Δ agr Δ pbp4/EDIII and RN4220 Δ agr Δ pbp3 Δ pbp4/EDIII, were remarkably decreased compared to the parent strain (Figure S3). However, the inactivation of alternative PBP3 and/or PBP4 substantially increased EV production (Figure 2d–f). Bradford protein measurement and EV particle detection indicated that the simultaneous deletion of *pbp3* and *pbp4* achieved a synergistic role in the EV secretion of *S. aureus*. The yield of Δ agr Δ pbp3 Δ pbp4 EVs was significantly higher than those of Δ agr Δ pbp3 EVs and Δ agr Δ pbp4 EVs ($p < 0.001$), and the production of Δ agr Δ pbp3 Δ pbp4 EVs was 4.64 ± 0.86 and 4.94 ± 0.17 times higher than that of Δ agr EVs in protein determination and EV particle counting, respectively (Figure 2e,f). These results suggested that PBP emerged as a crucial factor to affect *S. aureus* EV production and that deletion of alternative *pbp* genes was a promising strategy to enhance EV yield.

Given that β -lactam antibiotic treatment and *pbp3/pbp4* deletion improved EV production in *S. aureus*, TEM was performed to detect morphological changes of the bacteria under OXA treatment or after PBP inactivation. As shown in Figure 2g, bacterial cells of RN4220 Δ agr/EDIII exhibited normal morphological features with smooth and round cell walls. By contrast, abnormal morphological structures such as bacterial ghosts, disrupted cell walls and deformed septa were frequently observed in *S. aureus* cells after OXA treatment (Figure 2h). Meanwhile, *S. aureus* strain RN4220 Δ agr Δ pbp3 Δ pbp4/EDIII mainly presented aberrant bacterial division (Figure 2i). However, the morphological characteristics of bacterial EVs from β -lactam-treated and *pbp3/pbp4*-deleted strains were comparable to those of RN4220 Δ agr/EDIII (Figure 2j–l). These results implied that OXA treatment and PBP deletion may employ diverse mechanisms to affect EV release in *S. aureus*.

3.3 | OXA-Promoted EV Production in *S. aureus* Was ROS-Dependent

Bacteria under antibiotic pressure can exhibit metabolic change and active stress response (Kohanski et al. 2007). RNA sequencing (RNA-seq) was performed to explore the effect of sub-MIC of OXA on *S. aureus* gene expression (Table S4). A total of 538 genes significantly changed their expression levels after OXA treatment (Figure 3a, FC > 1.2 or < 0.83 and $p < 0.05$), and the enrichment of bacterial stress-related genes was observed (Figure 3b). Numerous stress-related regulators such as SsaA, Rex and Fur were upregulated after OXA treatment. Moreover, the expression levels of oxidative damage-related genes, including universal stress genes (*NMK49_RS08080*, *NMK49_RS10170* and *NMK49_RS08055*), heat-shock protein genes (*danK*, *danJ*, *groES*, *groEL* and *clp*) and DNA/protein damage-repair genes (*dinB*, *mutS2*, *bcp*, *ahpC* and *cysK*), changed in *S. aureus* after treatment with OXA (Figure 3b). These data showed that β -lactam treatment resulted in a significant increase of oxidative stress pressure on *S. aureus*.

We next determined the percentage of ROS-positive RN4220 cells after treatment with sub-MICs of OXA for 1.5 h. As shown

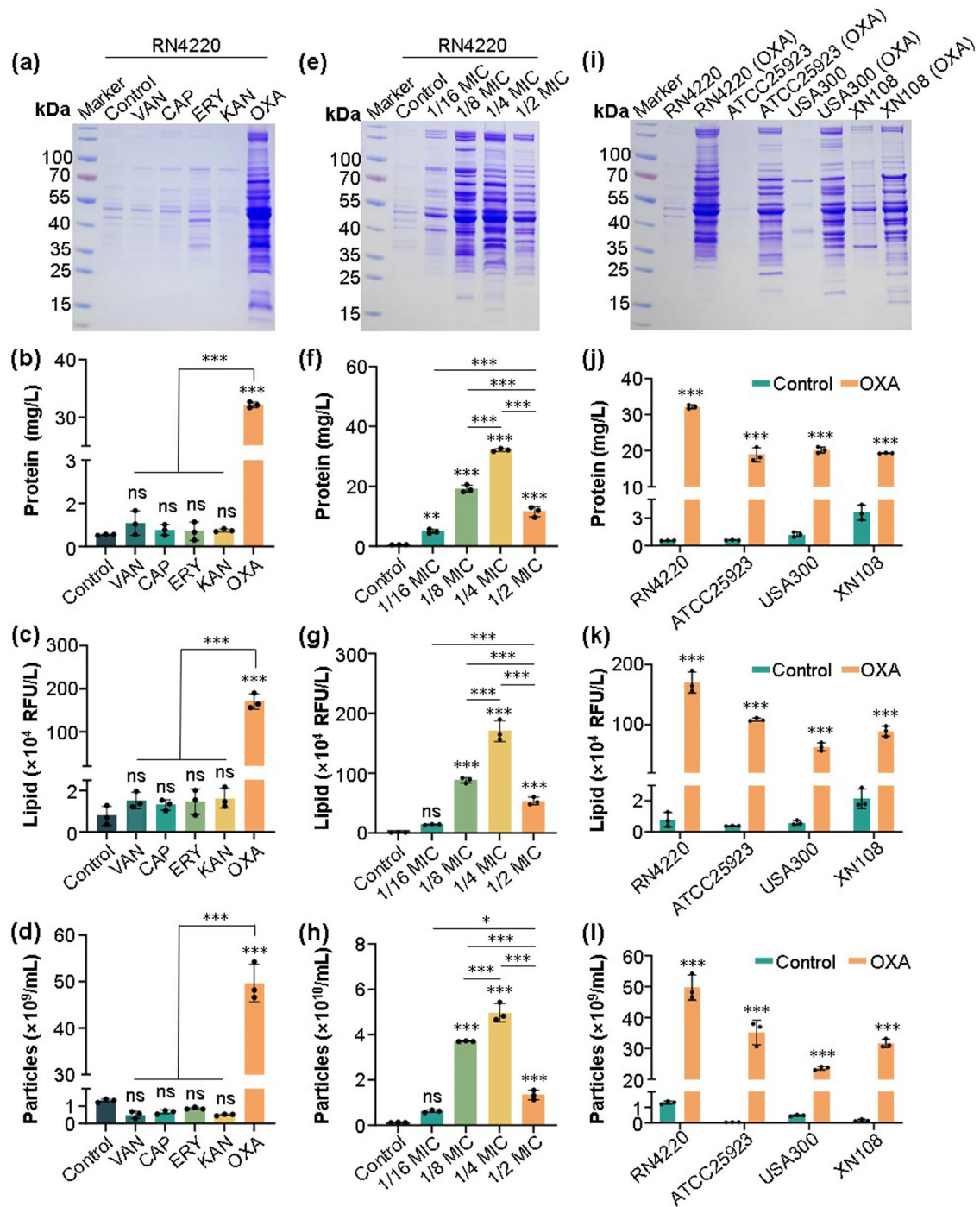


FIGURE 1 | Sub-MICs of β -lactam antibiotics enhanced EV production in *S. aureus*. (a) Representative SDS-PAGE analysis of EVs derived from *S. aureus* RN4220 treated with sub-MICs of various antibiotics. EVs derived from RN4220 without antibiotic treatment served as controls. The OXA-induced EV samples were twofold diluted before loading. The (b) protein and (c) lipid concentrations in the EV samples were determined using Broadband method and FM4-64 staining, respectively. (d) The particle numbers of different EV samples were analysed using resistive pulse sensing (RPS). (e) Representative SDS-PAGE analysis of EVs isolated from RN4220 treated with gradient concentrations of OXA. The 1/4 MIC of OXA-induced EV samples were twofold diluted before loading. Quantitative analysis of (f) protein, (g) lipid and (h) particle concentrations of EVs determined with Broadband method, FM4-64 staining and RPS, respectively. (i) Representative SDS-PAGE analysis of EVs purified from *S. aureus* strains with diverse genetic backgrounds, including MSSA strains RN4220 and ATCC25923, MRSA strain USA300, and VISA strain XN108, after treatment with or without 1/4 MIC of OXA. The antibiotic-induced EV samples were twofold diluted before loading. Quantitative analysis of (j) protein, (k) lipid and (l) particle contents in diverse EVs using Broadband method, FM4-64 staining and RPS, respectively. All experiments were performed in three biological replicates. Data are presented as mean \pm SD. The difference was evaluated by one-way ANOVA or unpaired *t*-test. * $p < 0.05$, ** $p < 0.01$, *** $p < 0.001$. ns indicates no statistical significance.

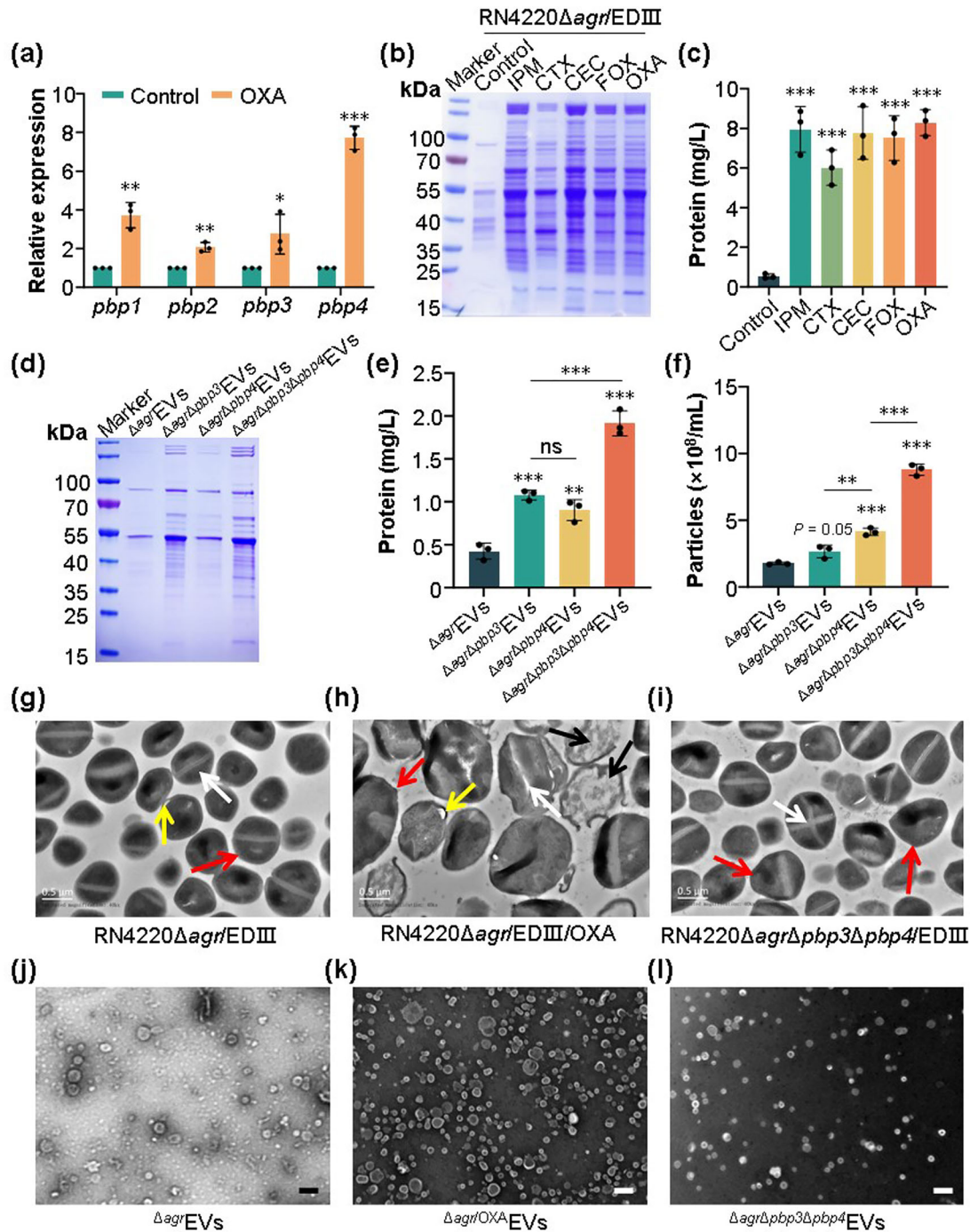


FIGURE 2 | Inactivation of alternative PBPs increased bacterial EV production in *S. aureus*. (a) RT-qPCR detection of the relative expression levels (normalised to the 16S rRNA gene) of *pbp1*, *pbp2*, *pbp3* and *pbp4* in *S. aureus* strain RN4220 Δ *agr*/EDIII with or without (control) OXA treatment. (b) Representative SDS-PAGE analysis of EVs derived from RN4220 Δ *agr*/EDIII treated with/without different β -lactams as indicated. The antibiotic-induced EV samples were twofold diluted before loading. (c) Quantitative analysis of protein concentrations in diverse EVs using Broadband method. (d) Representative SDS-PAGE analysis of EVs prepared from RN4220 Δ *agr*/EDIII and its derivatives with *pbp3* and/or *pbp4* gene deletion. (e) Protein concentrations and (f) particle counts in different EVs were analysed using Broadband method and RPS, respectively. Representative TEM pictures of (g) RN4220 Δ *agr*/EDIII, (h) RN4220 Δ *agr*/EDIII/OXA and (i) RN4220 Δ *agr* Δ *pbp3* Δ *pbp4*/EDIII. The smooth and folded cell walls are noted by the red arrows, whilst the white arrows indicate normal/abnormal bacterial separations, yellow arrows show protruded cell walls and black arrows point to disrupted cells. Representative TEM images of (j) Δ *agr*/EVs, (k) Δ *agr*/OXA EVs and (l) Δ *agr* Δ *pbp3* Δ *pbp4*/EVs. Scale bar, 200 nm. All experiments were performed for three biological replicates. Data are presented as mean \pm SD. Differences were evaluated by one-way ANOVA or unpaired *t*-test. **p* < 0.05, ***p* < 0.01, ****p* < 0.001. ns indicates no statistical significance.

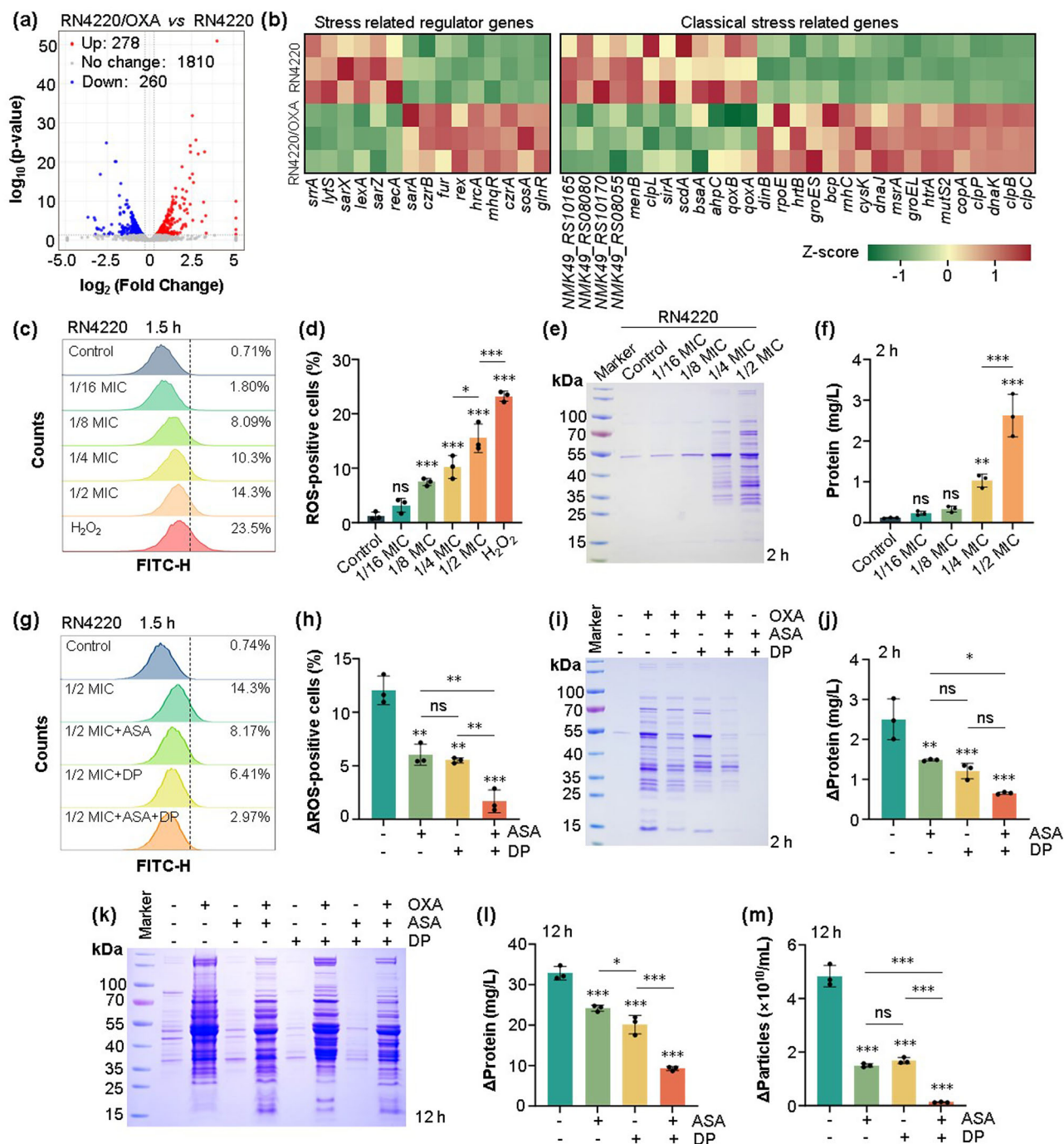


FIGURE 3 | Legend on next page.

in Figure 3c,d, ROS-positive bacterial cells increased with the increase of OXA concentrations. Meanwhile, the EV yields of *S. aureus* after diverse concentrations of OXA treatment were analysed with SDS-PAGE and Bradford method. A positive relationship was presented between OXA concentration and EV protein yield (Figure 3e,f). This dose-dependent promotion effect of OXA on ROS and EV generation was further confirmed with engineered *S. aureus* strain RN4220Δagr/EDIII (Figure S4), suggesting that OXA could promote EV production via intercellular ROS generation.

If OXA-induced EV production was ROS dependent, the application of ROS scavenger and/or inhibitor would impair the enhancement of OXA on EV secretion. As expected, the addition of either ASA or DP effectively decreased the percentage of ROS-positive cells (Figure 3g,h) and EV yields (Figure 3i,j) after treatment with 1/2 MIC of OXA. ASA and DP also exhibited a synergistic inhibitory effect on OXA-stimulated ROS generation and EV release (Figure 3h,j). The inhibitory effect of ROS antagonists on the OXA-enhanced EV production could be detected after 12 h of incubation (Figure 3k-m). These results suggested that ROS

participated in the process of sub-MIC β -lactam stimulating EV secretion.

3.4 | Deficiency of Redundant PBPs Triggered the Promotion Effect of β -Lactam Antibiotics on ROS and EV Production

Considering that PBPs and ROS were involved in the EV production of *S. aureus*, we wondered whether the deficiency of redundant PBPs would affect the effect of β -lactams on ROS and EV generation. Since 1/2 and 1/4 MICs of OXA considerably suppressed the growth of *S. aureus* RN4220 (Figure S1), therefore, a lower concentration of OXA (0.0156 $\mu\text{g/mL}$) was used, which represented 1/8 or 1/16 MIC of OXA against *S. aureus* strains of interest (Table S3). Equal numbers of *S. aureus* strains RN4220 Δagr /EDIII, RN4220 $\Delta\text{agr}\Delta\text{pbp3}$ /EDIII, RN4220 $\Delta\text{agr}\Delta\text{pbp4}$ /EDIII and RN4220 $\Delta\text{agr}\Delta\text{pbp3}\Delta\text{pbp4}$ /EDIII were inoculated in BHI media with 0.0156 $\mu\text{g/mL}$ of OXA and cultured at 37°C. After 2.5 h of OXA treatment, the ROS-positive *S. aureus* cells were evaluated with flow cytometry. The results demonstrated that the ROS productions in all strains enhanced after OXA treatment compared to their untreated controls, and *pbp4* deletion further increased the promotion effect of OXA on ROS (Figure 4a,b). The absolute differences in ROS production of the strains before and after OXA treatment were compared. Deletion of *pbp3* significantly increased the percentage of ROS-positive cells ($p < 0.01$), whereas *pbp4* deficiency slightly enhanced the ROS-positive cell numbers compared with its parent strain RN4220 Δagr /EDIII (Figure 4a,c). Double deletion of *pbp3* and *pbp4* jointly increased the level of OXA-triggered ROS (Figure 4c). These results indicated that the deficiency of redundant PBPs promoted OXA-induced ROS generation in *S. aureus*.

Next, bacterial EVs were prepared from the supernatants of *S. aureus* strains 3.5 h after OXA treatment. SDS-PAGE, EV protein concentration, and particle number counting revealed substantial increases in the EV yields of RN4220 $\Delta\text{agr}\Delta\text{pbp3}$ /EDIII and RN4220 $\Delta\text{agr}\Delta\text{pbp4}$ /EDIII relative to that of the RN4220 Δagr /EDIII (Figure 4d–f). Double inactivation of

pbp3 and *pbp4* resulted in even higher EV production, consistent with the trends of ROS levels (Figure 4c,e,f). Similar results were achieved in the *S. aureus* strains 12 h after OXA treatment (Figure 4g–i). Overall, these results suggested that inactivation of redundant PBPs enhanced the promotion effect of sub-MIC of β -lactams on ROS and EV production.

3.5 | ROS-Triggered Lipid Metabolic Reprogramming Mediated the OXA-Induced EV Production

It has been considered that EVs of Gram-positive bacteria are originally bubbling from bacterial cell membranes (Bitto et al. 2021b). We speculated that the change of bacterial membrane lipids could affect the EV production of Gram-positive bacteria. ROS can cause LPO and cell membrane dysfunction (Wang et al. 2022). Therefore, we detected the LPO level of *S. aureus* RN4220 cells after OXA treatment. Flow cytometry revealed that OXA enhanced the LPO levels of *S. aureus* in a dose-dependent manner, except for 1/2 MIC of OXA (Figure 5a,b). However, OXA-induced LPO levels remarkably decreased after the addition of ROS antagonists (Figure 5c,d). Similarly, LPO levels of the bacterial EVs were also dose-dependently enhanced by sub-MIC of OXA (Figure 5e), whereas the effects were blocked by adding ROS antagonists (Figure 5f). These data indicated that OXA treatment increased the LPO levels in *S. aureus* and its EVs, and ROS antagonists attenuated the OXA-enhanced LPO levels.

LPO may initiate antioxidant and membrane-repair mechanisms of bacteria (dos Anjos et al. 2023). Therefore, we performed transcriptomic analysis to evaluate the influence of OXA on bacterial lipid metabolism. GSEA enrichment revealed that several lipid metabolism pathways, including fatty acid biosynthesis, glycerolipid (GL) metabolism and glycerophospholipid metabolism, were altered after OXA treatment (Figure S5). Bacterial lipid synthesis initiates in a FASII module, which produces the primer and building blocks to support the elongation module that represents the central machinery of FASII enzymes (Parsons and Rock 2013, Figure 5g). Notably, RNA-seq revealed that OXA treatment upregulated several lipid biosynthesis-associated

FIGURE 3 | ROS played critical roles in β -lactam-promoted EV secretion in *S. aureus*. (a) RNA-seq analysis of differentially expressed genes between RN4220/OXA and RN4220. The volcano plot showed upregulated (red) and downregulated (blue) genes in RN4220/OXA versus RN4220. (b) Heat map showing the expression levels of stress-related genes in RN4220/OXA versus RN4220 of three independent samples. The data were normalised using Z-score. The colour scale ranges from -1.7 (green, lower than the average expression level) to $+1.4$ (red, higher than average expression level), and the pale-yellow represents Z-score = 0. The colour ruler covers all data ranges. (c) Flow cytometry detection of ROS-positive *S. aureus* RN4220 cells after treatment with different sub-MICs of OXA for 1.5 h. H_2O_2 (0.3%) was used as a positive control. (d) Comparison of ROS-positive *S. aureus* cells after OXA treatment. (e) Representative SDS-PAGE analysis of protein profiles in EVs derived from RN4220 treated with diverse sub-MICs of OXA for 2 h. (f) Comparison of protein concentrations in EVs. (g) Flow cytometry detection of ROS-positive RN4220 cells after treatment with OXA and ROS antagonists for 1.5 h. The ROS antagonists, ASA (10 mM) and DP (0.25 mM), were used in combination with 1/2 MIC of OXA in RN4220 culture. (h) Comparison of the Δ ROS-positive bacterial cells after flow cytometry analysis. RN4220 was cultured in BHI medium supplemented with 1/2 MIC of OXA, 10 mM ASA or/and 0.25 mM DP for 1.5 h. Δ ROS-positive cells = ROS-positive cells in OXA-treated group—ROS-positive cells in the control group. (i) Representative SDS-PAGE analysis of EV protein profiles after treatment with OXA and ROS antagonists for 2 h. (j) Comparison of Δ protein concentrations in the EVs derived from RN4220 treated with or without OXA and ROS antagonist. Δ Protein = Protein concentrations in the EVs prepared from OXA/ROS antagonist-treated group—Protein concentrations in the EVs from untreated control group. (k) Representative SDS-PAGE analysis of the EVs derived from RN4220 treated with or without OXA and ROS antagonist for 12 h. Comparison of (l) Δ protein and (m) Δ particle concentrations in EVs derived from RN4220 treated with or without OXA and ROS antagonist for 12 h. Δ Particles = Particle numbers of EVs from the OXA/ROS antagonist-treated group—Particle counts of EVs from the control group. All experiments were performed three times. Data are presented as mean \pm SD. The statistical difference was evaluated by one-way ANOVA. * $p < 0.05$, ** $p < 0.01$, *** $p < 0.001$. ns indicates no statistical significance.

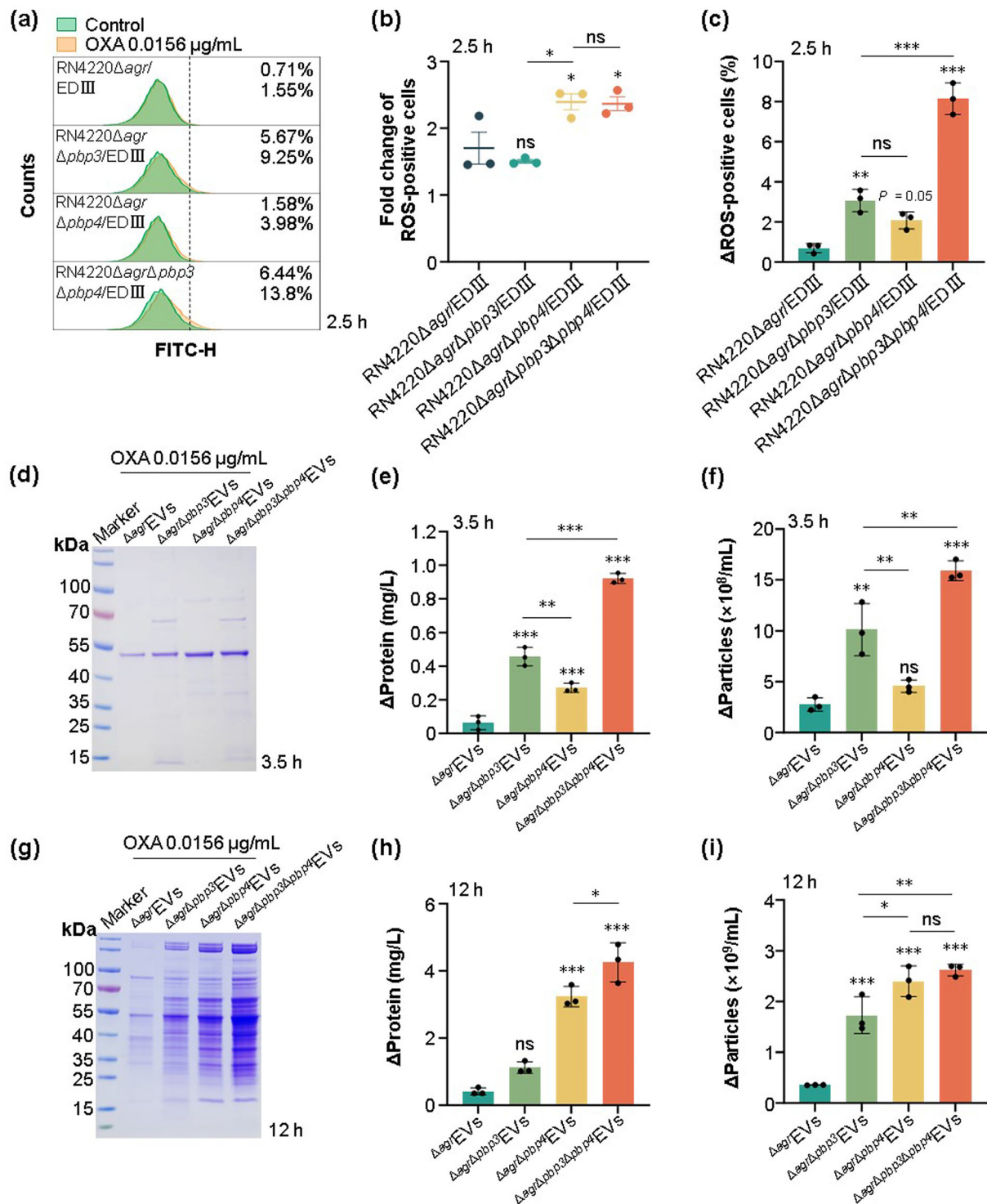


FIGURE 4 | Inactivation of redundant PBPs increased the effects of OXA on ROS and EV production in *S. aureus*. (a) Flow cytometry detection of ROS-positive cells of RN4220 Δagr /EDIII and its derivatives with or without OXA-treatment. Equal numbers of *S. aureus* RN4220 Δagr /EDIII and its derivatives were respectively inoculated and cultured in BHI medium with or without 0.0156 $\mu\text{g/mL}$ of OXA for 2.5 h, bacterial cells were harvested and the percentage of ROS-positive cells was analysed. (b) Fold change of ROS-positive cells in the OXA-treated bacteria compared with those in the untreated control cells. (c) Comparison of ΔROS -positive bacterial cells after flow cytometry analysis. ΔROS -positive cells = The percentage of ROS-positive cells after OXA treatment—The percentage of ROS-positive cells without OXA treatment. *S. aureus* RN4220 Δagr /EDIII and its derivatives were treated with/without OXA (0.0156 $\mu\text{g/mL}$) for 3.5 h. Bacterial EVs were harvested. (d) Protein profiles, (e) protein concentrations and (f) particle numbers were evaluated by SDS-PAGE, Broadband method and RPS, respectively. (g) Protein profiles, (h) protein concentrations and (i) particle counts of EVs from *S. aureus* RN4220 Δagr /EDIII and its derivatives treated with/without OXA (0.0156 $\mu\text{g/mL}$) for 12 h. $\Delta\text{Protein}$ = Protein concentrations of EVs from the OXA-treated group—Protein concentrations of EVs from the control group. $\Delta\text{Particle}$ = Particle counts of EVs from the OXA-treated group—Particle numbers of EVs from the control group. All experiments were performed three times. Data are presented as mean \pm SD. The statistical difference was evaluated by one-way ANOVA. * $p < 0.05$, ** $p < 0.01$, *** $p < 0.001$. ns indicates no statistical significance.

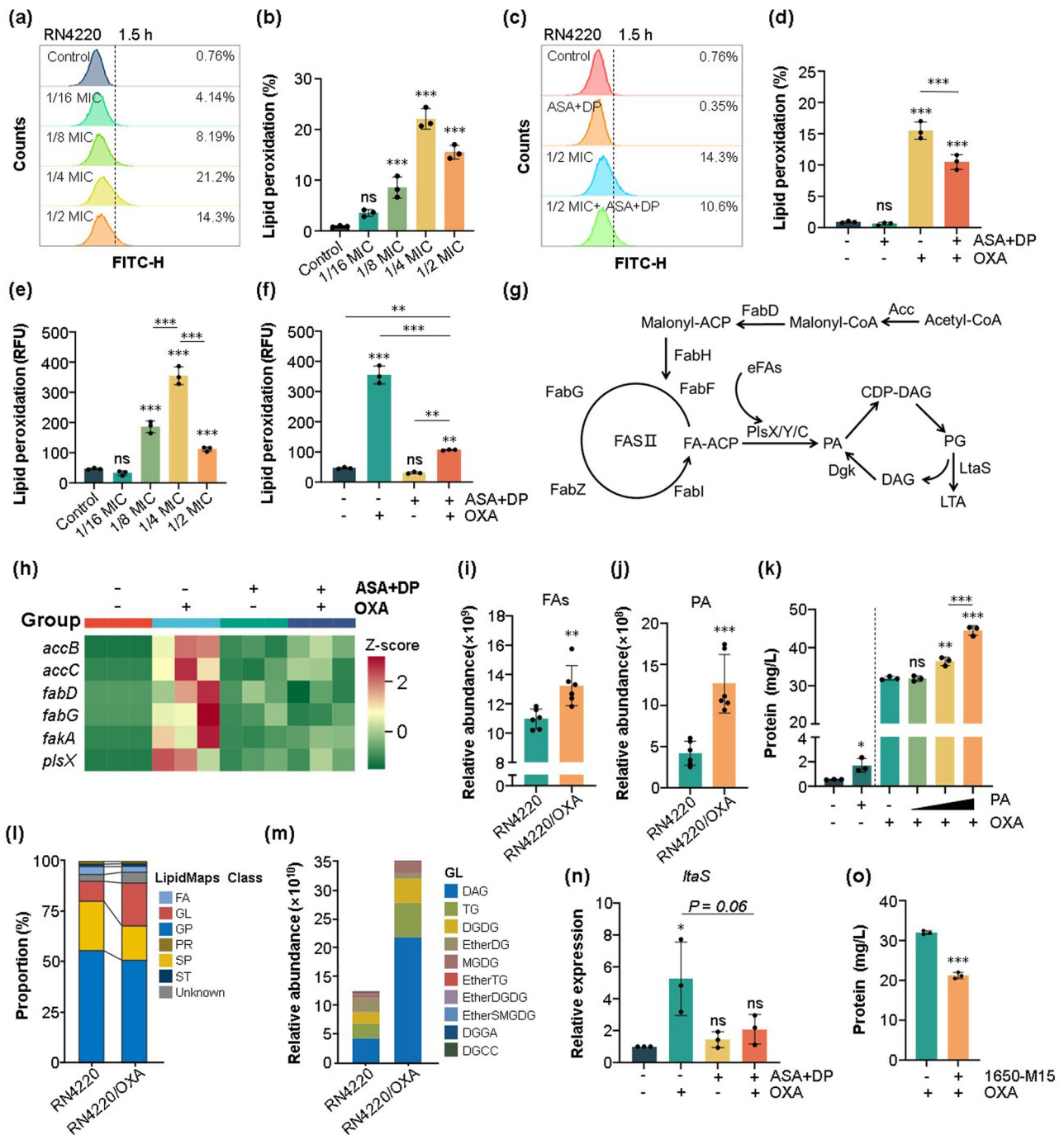


FIGURE 5 | Legend on next page.

genes, including *accB*, *accC*, *fabD*, *fabG*, *fakA* and *plsX* (Table S4). RT-qPCR confirmed the stimulatory effect of OXA on the expression levels of these genes (Figure 5h), and such effect could be suppressed by the addition of ROS antagonists. Moreover, non-targeted lipidomic analysis was performed (Table S5), and the results revealed a substantial increase of fatty acids (FAs) in *S. aureus* RN4220 after OXA exposure (Figure 5i). The increasing of FAs can promote the generation of PA, one important precursor for the synthesis of lipids (Parsons and Rock 2013). As expected, PA production significantly increased in RN4220 treated with OXA compared with that in the untreated strain ($p < 0.001$, Figure 5j).

If ROS-triggered PA synthesis contributed to OXA-stimulated EV production in *S. aureus*, the exogenous addition of PA would play a role. As shown in Figure S6, PA only posed a negligible influence on bacterial growth unless OXA was added. Notably, the addition of 4 $\mu\text{g/mL}$ of PA considerably enhanced the EV production of *S. aureus* RN4220 without OXA treatment ($p < 0.05$); moreover, PA exhibited a dose-dependent promotion effect on the EV yield of RN4220 under OXA stress (Figure 5k). On the contrary, the addition of cardiolipin (CL), which was also promoted by OXA (Figure S7a), even inhibited the EV production of the *S. aureus* RN4220 (Figure S7b), whereas the bacterial growth was promoted (Figure S7c). Since PA is a lipid precursor

(Parsons and Rock 2013), we wondered which downstream lipids of PA played roles in promoting bacterial EV yields. The lipidomic data were analysed, and a substantial increase of GL in *S. aureus* after OXA treatment was observed (Figure 5l). Among GL, diacylglycerol (DAG) was the highest increased lipid (34.4% vs. 62.1%) detected in *S. aureus* after OXA exposure (Figure 5m). DAG is a key bypass product of LTA synthesis (Percy and Gründling 2014). Accordingly, the expression level of LTA synthetic gene *ltaS* remarkably increased in *S. aureus* with OXA treatment, and such an effect was inhibited by the addition of ROS antagonists ASA and DP (Figure 5n). Moreover, the addition of LtaS enzyme inhibitor, 1650-M15, substantially suppressed EV production in *S. aureus* under OXA exposure (Figure 5o), whilst the bacterial replication was not affected (Figure S8). Collectively, these results suggested that the OXA-induced ROS could reprogram *S. aureus* lipid metabolism, which augmented the biosynthesis of PA and LTA to promote EV production.

3.6 | OXA Exposure Affected the Property and Immunogenicity of *S. aureus* EVs

Change in the cultural condition of bacteria may alter the properties of bacterial EVs (Ye et al. 2021; Chen et al. 2023). The morphological features of EVs derived from OXA-treated RN4220 Δ agr/EDIII (Δ agr/OXA EVs), RN4220 Δ agr/EDIII (Δ agr EVs) and RN4220 Δ agr Δ pbp3 Δ pbp4/EDIII (Δ agr Δ pbp3 Δ pbp4 EVs) were observed under TEM, and these EVs displayed typical double-layer membrane structures (Figure 2j–l). Moreover, RPS revealed that Δ agr EVs (68 ± 17.8 nm), Δ agr Δ pbp3 Δ pbp4 EVs (68 ± 14.5 nm) and Δ agr/OXA EVs (66 ± 11.1 nm) presented comparable particle sizes (Figure 6a). Proteomic analysis identified a total of 260 proteins from the purified EVs (Figure 6b). Among these, only 41 proteins were shared by Δ agr EVs, Δ agr Δ pbp3 Δ pbp4 EVs and Δ agr/OXA EVs (Figure 6b and Table S6). These data suggested that the treatment with OXA contributed to comparable particle sizes and changed the protein contents of *S. aureus* EVs. However,

the function of EVs derived from *S. aureus* after OXA treatment required experimental verification.

S. aureus RN4220 Δ agr/EDIII was engineered to carry DENV EDIIIconA and EDIIIconB antigens to bacterial Δ agr EVs (Yuan et al. 2018). Western blot confirmed the successful loading of EDIIIconA/B antigens in the Δ agr/OXA EVs, Δ agr EVs and Δ agr Δ pbp3 Δ pbp4 EVs (Figure 6c), with Δ agr/OXA EVs carrying the most amount of EDIIIconB antigen (Figure 6d). Next, BALB/c mice were intraperitoneally injected with equal amounts of purified EVs to assess their immunological functions (Figure 6e). The body weights of the immunised mice changed similarly to that of the PBS control (Figure S9). After 6 h of primary immunisation, sera were collected and inflammatory cytokines were detected by ELISA. The results indicated that EV immunisation remarkably increased the levels of inflammatory cytokines IL-6 and TNF- α compared with the PBS control, except for TNF- α in the Δ agr Δ pbp3 Δ pbp4 EV-challenged mice (Figure 6f, g). Three weeks after the last boosting, blood samples were obtained and subjected to EDIII-specific antibody detection. As shown in Figure 6h–j, the titres of EDIII-specific IgG, IgG1 and IgG2a in mice injected with Δ agr Δ pbp3 Δ pbp4 EVs reached 10^3 , 10^5 and 10^4 , respectively, which were similar to those of mice immunised with Δ agr EVs. By contrast, the Δ agr/OXA EV inoculation stimulated even higher antibody titres of IgG (10^5), IgG1 (10^6) and IgG2a (10^5). Taken together, these results suggested that OXA exposure strengthened the immune property of *S. aureus* EVs with an equal amount of total protein, implying a promising strategy for engineered bacterial-EV preparation.

4 | Discussion

Most studies on bacterial EVs have focused on Gram-negative bacteria, and EV production of Gram-positive bacteria has only recently been demonstrated (Lee et al. 2009; Andreoni et al. 2019). The main purpose of this study was to explore ways to promote EV production in Gram-positive *S. aureus*. We showed that only

FIGURE 5 | OXA-induced ROS triggered lipid metabolic reprogramming to increase EV production in *S. aureus*. (a) Flow cytometry detection of LPO levels of *S. aureus* RN4220 treated with different sub-MICs of OXA for 1.5 h. (b) Comparison of LPO levels of RN4220 after OXA treatment. (c) Flow cytometry detection of LPO levels of RN4220 treated with or without 1/2 MIC of OXA and ROS antagonists (ASA and DP) for 1.5 h. (d) Comparison of LPO levels of RN4220 after treatment with OXA and ROS antagonists. (e) Comparison of LPO levels of EVs derived from RN4220 treated with diverse concentrations of OXA for 12 h. (f) Comparison of LPO levels of EVs derived from RN4220 treated with 1/2 MIC of OXA and ROS antagonists for 12 h. (g) Schematic diagram showing metabolic pathways involved in FAs, PA and LTA synthesis. (h) Heat map of RT-qPCR detection of lipid metabolic related genes. Data show the relative expressional levels of target genes in *S. aureus* treated with or without OXA and ROS antagonists. The 16S rRNA gene was used as a reference. The relative expressional levels of target genes were normalised by Z-score. The colour scale ranges from -1.1 (green, lower than the average expression level) to +2.8 (red, higher than the average expression level), and the pale-yellow represents Z-score = 0. The colour ruler covers all data ranges. Comparison of (i) FAs and (j) PA contents by non-targeted lipidomic analysis in RN4220 with or without OXA treatment for 2 h. (k) Protein concentrations of EVs from *S. aureus* under normal conditions and OXA stress with/without the addition of exogenous PA (0.04, 0.4 and 4 μ g/mL). (l) Lipid categories and their proportions in the total lipids after lipidomic analysis. (m) Top 10 lipid class in the GL category after lipidomic analysis. (n) RT-qPCR detection of *ltaS* expression in RN4220 treated with or without OXA and ROS antagonists. The expression data were normalised to the 16S rRNA gene. (o) Protein concentrations of EVs from RN4220 treated with 1/4 MIC of OXA and/or LtaS inhibitor (1650-M15, 10 μ M). Bacterial EVs were harvested, and protein concentrations were detected by the Broadband method. All experiments were performed three times. Data are presented as mean \pm SD. The statistical difference was evaluated by one-way ANOVA or unpaired *t*-test. **p* < 0.05, ***p* < 0.01, ****p* < 0.001. CDP-DAG indicates cytidine diphosphate-diacylglycerol; DAG, diacylglycerol; DGCC, DAG-3-O-carboxyhydroxymethylcholine; DGDG, digalactosyl-DAG; DGGa, DAG glucuronide; eFAs, exogenous FAs; EtherDG, ether-linked diacylglycerol; EtherDGDG, ether-linked DGDG; EtherSMGDG, ether-linked semino-MGDG; EtherTG, Ether-linked TAG; FA, fatty acyls; FAs, fatty acids; FAs-ACP, FAs-acyl carrier protein; GL, glycerolipids; GP, glycerophospholipids; LTA, lipoteichoic acid; MGDG, monogalactosyl-DAG; ns, no statistical significance; PA, phosphatidic acid; PG, phosphatidylglycerol; PR, prenol lipids; SP, sphingolipids; ST, sterol lipids; TAG, triacylglycerol.

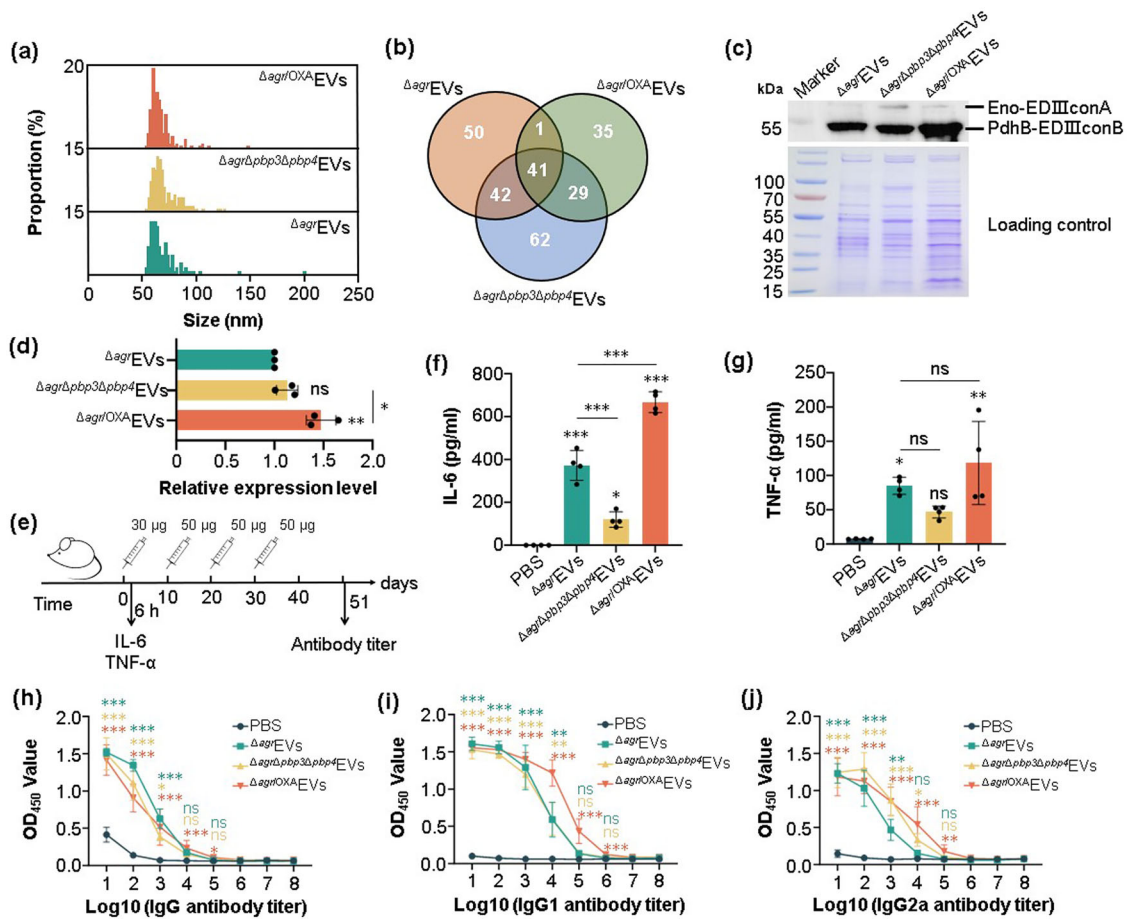


FIGURE 6 | OXA-treatment altered *S. aureus* EV property and immunogenicity. (a) Particle distribution of bacterial EVs determined using RPS. (b) Venn diagram showing EV-loaded protein numbers after proteomic analysis. (c) Representative Western blot analysis of the loaded Eno-EDIIIconA and PdhB-EDIIIconB proteins in EVs. The mouse anti-EDIII specific antibodies (DENV-2, mainly against EDIIIconB) were used as the first antibody, and HRP-conjugated goat anti-mouse antibody was used as the secondary antibody. Coomassie stained SDS-PAGE gel was used as loading control. (d) Comparison of the relative expression levels of EDIIIconB in EVs. The grey values of protein bands in the Western blot were evaluated by ImageJ software and normalised to the grey values of corresponding SDS-PAGE gels. The relative grey value of Δagr EVs was set as 1.0. (e) Schematic diagram showing the immunising strategy in animal experiments. BALB/c mice were intraperitoneally injected with diverse amounts of EVs as indicated at certain time points. Serum samples were collected 6 h after the primary immunisation, and the levels of (f) IL-6 and (g) TNF- α were detected by ELISA ($n = 5$). Mice were sacrificed 21 days after the last injection and serum samples were collected. The titres of Dengue EDIII-specific (h) IgG, (i) IgG1 and (j) IgG2a were detected ($n = 5$). The data are presented as mean \pm SD. The statistical difference was evaluated by one-way ANOVA. * $p < 0.05$, ** $p < 0.01$, *** $p < 0.001$. ns indicates no statistical significance.

β -lactams such as OXA, IMP, CTX, CEC and FOX, but not VAN, CAP, ERY and KAN, enhanced EV production in *S. aureus* with diverse genetic backgrounds (Figure 1). Although the treatment of bacteria with β -lactam antibiotics is an effective trigger for bacterial EV production (Wang et al. 2018; Kim et al. 2020), the underlying mechanisms remain poorly understood. We demonstrated that both PBP proteins and ROS molecules were involved in the process of β -lactam-promoted bacterial EV production (Figures 2 and 3). Previous studies showed that inactivation of PBP encoding genes increased bacterial EV production (Nevermann et al. 2019; Giacomucci et al. 2022). Herein, we found that inactivation of alternative PBP3 and/or PBP4 could increase EV production of the *S. aureus* RN4220 Δagr /EDIII under sub-MICs of OXA exposure. Given that the expression levels of bacterial stress-related genes changed in the *S. aureus* strain RN4220 after treatment with OXA, we hypothesised that the endogenous ROS generated under antibiotic stress was involved in OXA-triggered

EV production. As expected, the percentage of ROS-positive *S. aureus* cells increased gradually with the increase of OXA concentrations, and the addition of ROS scavenger ASA and/or inhibitor DP arrested the OXA-stimulated ROS generation, and resulted in decreased EV yields under β -lactam stress. Notably, the increasing EV production was highly consistent with the elevated ROS level in *S. aureus* with OXA treatment, indicating the participation of ROS in the process of OXA-induced EV yields. However, even when using ASA and DP in combination, sub-MIC of OXA exposure stimulated more EVs in *S. aureus*, suggesting the possible involvement of additional factors such as weakened peptidoglycan layer and reduced cell wall cross-linking in the β -lactam-triggered EV production (Wang et al. 2018; Andreoni et al. 2019).

Interestingly, we found that PBPs could affect endogenous ROS production (Figure 4a,b). Inactivation of PBP3 and PBP4

strengthened the inducing effect of β -lactams on ROS, and further increased EV production in *S. aureus* (Figure 4). PBP molecules are the targets of β -lactams like OXA. We speculated that β -lactams acted on PBPs and triggered a futile cycle of peptidoglycan synthesis, which led to more degradation of peptidoglycan in *S. aureus* (Cho et al. 2014). These phenomena can cause bacterial toxic metabolism reflected in abnormalised central carbon, amino acid and nucleic acid metabolisms, thereby further altering respiratory and energy utilisation to induce ROS accumulation (Belenky et al. 2015; Léger et al. 2019; Lobritz et al. 2022). In this study, various genes related to central carbon metabolism, amino acid metabolism and electronic-transfer chain (ubiquinone biosynthesis pathway) were enriched in OXA-treated *S. aureus* (Figure S10). In the case of *pbp3* and *pbp4* deletion, more β -lactam molecules turned to target PBP1 and PBP2, which are enzymes crucial for bacterial cell-wall biogenesis. The redirection of β -lactams intensified the deficiency of cell wall synthesis and induced stronger oxidative stress in the intracellular environments.

We confirmed that the OXA-induced EV production in *S. aureus* was ROS dependent. However, the mechanism underlying intracellular ROS-enhanced bacterial EV production was poorly understood. We proposed that the accumulated ROS in *S. aureus* after OXA exposure led to lipid metabolic reprogramming, which increased the biosynthesis of lipids PA and LTA to promote EV production. Firstly, the accumulated ROS could attack bacterial lipid components, resulting in an imbalance in membrane homeostasis. We observed that OXA treatment induced LPO of *S. aureus* cell membranes in a dose-dependent manner, and such role was inhibited by ROS antagonists. Moreover, the contents of membrane homeostasis-related lipids could be changed under OXA conditions (Parsons and Rock 2013; Sohlenkamp et al. 2016). Notably, lipidomics revealed the remarkably increased contents of monoglycosyl-DAG (MGDG) and diglycosyl-DAG (DGDG) and most decreased lysophospholipids such as lysophosphatidylcholine (LPC), lysophosphatidylinositol (LPI), lysophosphatidylserine (LPS) and lysophosphatidylglycerol (LPG) in the OXA-treated *S. aureus* cells (Figure S11). Secondly, bacterial self-renewal mechanism could be activated by the damaged membrane components. FAs and PA are crucial precursors for lipid biosynthesis (Parsons and Rock 2013). We noticed that the expression levels of genes involved in FAs and PA synthesis such as *accB*, *fabG* and *plsX* increased, which resulted in elevated FAs and PA contents to facilitate membrane repairing in *S. aureus* after OXA treatment. Thirdly, increased PA contents could boost the synthesis of downstream lipids contributing to bacterial EV secretion. The addition of exogenous PA promoted EV production, and this effect was even stronger in *S. aureus* under OXA induction. The downstream PA lipids such as DAG (a bypass product during LTA synthesis) and the LTA synthetic gene *ltaS* level considerably increased in *S. aureus* after OXA treatment. LTA is a negative-charged substance of Gram-positive *S. aureus* (Percy and Gründling 2014). It has been reported that the accumulation of negative-charged lipopolysaccharides in the periplasm of Gram-negative bacteria can alter membrane characteristics and promote vesicle release (Schwechheimer and Kuehn 2015; McMillan and Kuehn 2021). Therefore, we supposed that LTA could also involve in EV production of *S. aureus*. Experimentally, the addition of LtaS inhibitor (1650-M15) remarkably decreased OXA-triggered EV production. Besides, the conical shape lipids

like PA and DAG are reported to increase the curvature of cell membrane (Agrawal and Ramachandran 2019), and such action could also mediate the OXA-induced *S. aureus* EV secretion. Finally, the secretion of EVs could carry the dysfunctional lipids away, and facilitate the growth of bacterial cells under antibiotic stress. Deng et al. (2024) reported that *Coscinodiscus radiatus* can trigger extracellular EV production to remove harmful metabolites. In this study, we not only detected the enrichment of LPO in the OXA-induced EVs, but also observed an elevation of ROS levels within EVs derived from *S. aureus* cells after treatment with OXA (Figure S12). However, the fine action of OXA stress in the increased EV release of *S. aureus* needs further investigation.

The impact of OXA treatment on the components and immunological functions of bacterial EVs was primarily elucidated. We have reported that deleting the *hld* gene in *S. aureus* results in slightly enlarged EV particle sizes and more kinds of EV cargo proteins (Chen et al. 2023). Here, changes in EV-loaded proteins were also observed in the OXA-treated *S. aureus* strains compared with the control (Figure 6a–c). However, BALB/c mice immunised with diverse EVs with identical total proteins revealed that OXA-induced $\Delta_{agr/OXA}$ EVs stimulated higher levels of Dengue EDIII-specific antibodies than the control groups (Figure 6k–m). This phenomenon may be ascribed to the elevated EDIII antigen loading in the EVs or β -lactam-induced EV adjuvant that activates immune responses. Certain *S. aureus* contents, such as LTA, can bind toll-like receptor 2 to induce proinflammatory production and trigger immune responses (Kimbrell et al. 2008; Yamasaki-Yashiki et al. 2024). In addition, $\Delta_{agr/OXA}$ EVs had more particles than Δ_{agr} EVs and $\Delta_{agr\Delta pbp3\Delta pbp4}$ EVs with equal total proteins (Figure S13), and the appropriate EV particles may facilitate the uptake and presentation of certain antigens. Overall, the mechanism underlying the enhanced immunogenicity of the OXA-triggered EVs is unclear and needs to be further studied.

In conclusion, this study uncovered a PBP-limited ROS-dependent mechanism for β -lactam-promoted EV production in *S. aureus*. The effect of β -lactams on EV immunological functions was also evaluated. Our results provided a feasible solution to improve EV production in *S. aureus*. Further study in this field may lead to the mechanic insights into antibiotic-induced bacterial EV secretion and innovative strategies to prepare EVs for application.

Author Contributions

Xiaonan Huang: investigation(lead), methodology(lead), resources(equal), writing–original draft(Equal), Writing – review and editing(equal). **Zhen Hu:** investigation, formal analysis, methodology, resources, visualisation, writing–original draft, writing–review and editing. **Weilong Shang, Juan Chen, Qiwen Hu and Mengyang Li:** formal analysis, investigation, methodology. **Jing Yin:** formal analysis(Equal), methodology(Equal). **Yumin Zhou, Ruolan Ding, He Liu, Jianxiong Dou, Huagang Peng, Yifan Rao, Lu Liu, Yuting Wang, Li Tan, Yuhua Yang, Jianghong Wu and Chuan Xiao:** formal analysis, methodology. **Yi Yang:** conceptualisation, formal analysis, investigation, methodology, project administration, supervision, validation, writing–original draft, writing–review and editing. **Xiancai Rao:** conceptualization(lead), data curation(lead), formal analysis(equal), funding acquisition(Lead), supervision(Lead), validation(Equal), writing–review and editing(lead).

Acknowledgements

This work was supported by the National Natural Science Foundation of China (No. 82071857). The funders had no role in study design, data collection and analysis, decision to publish or preparation of the manuscript.

Conflicts of Interest

The authors declare no conflicts of interest.

Data Availability Statement

The RNA-seq and mass spectrometry proteomic data of all the strains used in this study are available in the SRA database and ProteomeXchange Consortium under accession numbers listed in Methods. Other relevant data supporting the findings presented are available within the paper and its Supporting materials.

References

- Abitbol, V., F. Martín-Torres, M.-K. Taha, et al. 2024. "4CMenB Journey to the 10-Year Anniversary and Beyond." *Human Vaccines & Immunotherapeutics* 20, no. 1: 2357924.
- Agrawal, A., and R. Ramachandran. 2019. "Exploring the Links Between Lipid Geometry and Mitochondrial Fission: Emerging Concepts." *Mitochondrion* 49: 305–313.
- Andreoni, F., M. Toyofuku, C. Menzi, et al. 2019. "Antibiotics Stimulate Formation of Vesicles in *Staphylococcus aureus* in Both Phage-Dependent and -Independent Fashions and via Different Routes." *Antimicrobial Agents and Chemotherapy* 63, no. 2: e01439–18.
- Belenky, P., J. D. Ye, C. B. M. Porter, et al. 2015. "Bactericidal Antibiotics Induce Toxic Metabolic Perturbations That Lead to Cellular Damage." *Cell Reports* 13, no. 5: 968–980.
- Bitto, N. J., L. Cheng, E. L. Johnston, et al. 2021a. "Staphylococcus aureus Membrane Vesicles Contain Immunostimulatory DNA, RNA and Peptidoglycan That Activate Innate Immune Receptors and Induce Autophagy." *Journal of Extracellular Vesicles* 10, no. 6: e12080.
- Bitto, N. J., L. Zavan, E. L. Johnston, T. P. Stinear, A. F. Hill, and M. Kaparakis-Liaskos. 2021b. "Considerations for the Analysis of Bacterial Membrane Vesicles: Methods of Vesicle Production and Quantification Can Influence Biological and Experimental Outcomes." *Microbiology Spectrum* 9, no. 3: e0127321.
- Briaud, P., A. Frey, E. C. Marino, et al. 2021. "Temperature Influences the Composition and Cytotoxicity of Extracellular Vesicles in *Staphylococcus aureus*." *mSphere* 6, no. 5: e0067621.
- Chen, J., Y. Lv, W. Shang, et al. 2023. "Loaded Delta-Hemolysin Shapes the Properties of *Staphylococcus aureus* Membrane Vesicles." *Frontiers in Microbiology* 14: 1254367.
- Chen, J., H. Zhou, J. Huang, R. Zhang, and X. Rao. 2021. "Virulence Alterations in *Staphylococcus aureus* Upon Treatment With the Sub-Inhibitory Concentrations of Antibiotics." *Journal of Advanced Research* 31: 165–175.
- Cho, H., T. Uehara, and T. G. Bernhardt. 2014. "Beta-lactam Antibiotics Induce a Lethal Malfunctioning of the Bacterial Cell Wall Synthesis Machinery." *Cell* 159, no. 6: 1300–1311.
- Collins, S. M., and A. C. Brown. 2021. "Bacterial Outer Membrane Vesicles as Antibiotic Delivery Vehicles." *Frontiers in Immunology* 12: 733064.
- Deng, Y., R. Yu, V. Grabe, et al. 2024. "Bacteria Modulate Microalgal Aging Physiology Through the Induction of Extracellular Vesicle Production to Remove Harmful Metabolites." *Nature Microbiology* 9, no. 9: 2356–2368.
- Domingues, S., and K. M. Nielsen. 2017. "Membrane Vesicles and Horizontal Gene Transfer in Prokaryotes." *Current Opinion in Microbiology* 38: 16–21.
- dos Anjos, C., L. G. Leanse, M. S. Ribeiro, et al. 2023. "New Insights Into the Bacterial Targets of Antimicrobial Blue Light." *Microbiology Spectrum* 11, no. 2: e0283322.
- Giacomucci, S., A. Mathieu-Denoncourt, A. T. Vincent, H. Jannadi, and M. Duperthuy. 2022. "Experimental Evolution of *Vibrio Cholerae* Identifies Hypervesiculation as a Way to Increase Motility in the Presence of Polymyxin B." *Frontiers in Microbiology* 13: 932165.
- Hodille, E., W. Rose, B. A. Diep, S. Goutelle, G. Lina, and O. Dumitrescu. 2017. "The Role of Antibiotics in Modulating Virulence in *Staphylococcus aureus*." *Clinical Microbiology Reviews* 30, no. 4: 887–917.
- Hu, K., E. Palmieri, K. Samnuan, B. Ricchetti, et al. 2022. "Generalized Modules for Membrane Antigens (GMMMA), an Outer Membrane Vesicle-Based Vaccine Platform, for Efficient Viral Antigen Delivery." *Journal of Extracellular Vesicles* 11, no. 11: e12247.
- Hu, Q., H. Peng, and X. Rao. 2016. "Molecular Events for Promotion of Vancomycin Resistance in Vancomycin Intermediate *Staphylococcus aureus*." *Frontiers in Microbiology* 7: 1601.
- Huang, W., L. Meng, Y. Chen, Z. Dong, and Q. Peng. 2022. "Bacterial Outer Membrane Vesicles as Potential Biological Nanomaterials for Antibacterial Therapy." *Acta Biomaterialia* 140: 102–115.
- Jeong, G.-J., F. Khan, N. Tabassum, K.-J. Cho, and Y.-M. Kim. 2024. "Bacterial Extracellular Vesicles: Modulation of Biofilm and Virulence Properties." *Acta Biomaterialia* 178: 13–23.
- Kaparakis-Liaskos, M., and R. L. Ferrero. 2015. "Immune Modulation by Bacterial Outer Membrane Vesicles." *Nature Reviews Immunology* 15, no. 6: 375–387.
- Kim, J. H., J. Lee, J. Park, and Y. S. Gho. 2015. "Gram-Negative and Gram-Positive Bacterial Extracellular Vesicles." *Seminars in Cell & Developmental Biology* 40: 97–104.
- Kim, O. Y., H. T. Park, N. T. H. Dinh, et al. 2017. "Bacterial Outer Membrane Vesicles Suppress Tumor by Interferon- γ -Mediated Antitumor Response." *Nature Communications* 8: 626.
- Kim, S. W., J.-S. Seo, S. B. Park, et al. 2020. "Significant Increase in the Secretion of Extracellular Vesicles and Antibiotics Resistance From Methicillin-Resistant *Staphylococcus aureus* Induced by Ampicillin Stress." *Scientific Reports* 10, no. 1: 995–1005.
- Kimbrell, M. R., H. Warshakoon, J. R. Cromer, et al. 2008. "Comparison of the Immunostimulatory and Proinflammatory Activities of Candidate Gram-Positive Endotoxins, Lipoteichoic Acid, Peptidoglycan, and Lipopeptides, in Murine and human Cells." *Immunology Letters* 118, no. 2: 132–141.
- Kohanski, M. A., D. J. Dwyer, B. Hayete, C. A. Lawrence, and J. J. Collins. 2007. "A Common Mechanism of Cellular Death Induced by Bactericidal Antibiotics." *Cell* 130, no. 5: 797–810.
- Lade, H., and J. S. Kim. 2023. "Molecular Determinants of β -Lactam Resistance in Methicillin-Resistant *Staphylococcus aureus* (MRSA): An Updated Review." *Antibiotics-Basel* 12, no. 9: 1362.
- Lee, E. Y., D. Y. Choi, D. K. Kim, et al. 2009. "Gram-Positive Bacteria Produce Membrane Vesicles: Proteomics-Based Characterization of *Staphylococcus aureus*-Derived Membrane Vesicles." *Proteomics* 9, no. 24: 5425–5436.
- Léger, L., A. Budin-Verneuil, M. Cacaci, A. Benachour, A. Hartke, and N. Verneuil. 2019. " β -Lactam Exposure Triggers Reactive Oxygen Species Formation in *Enterococcus faecalis* via the respiratory Chain Component DMK." *Cell Reports* 29, no. 8: 2184–2191.
- Li, M., Y. Wang, H. Liu, et al. 2024. "Staphylococcus aureus Membrane Vesicles Kill Tumor Cells Through a Caspase-1-Dependent Pyroptosis Pathway." *International Journal of Nanomedicine* 19: 4007–4019.
- Li, Y., X. Ma, Y. Yue, et al. 2022. "Rapid Surface Display of mRNA Antigens by Bacteria-Derived Outer Membrane Vesicles for a Personalized Tumor Vaccine." *Advanced Materials* 34, no. 20: e2109984.

- Liu, Y., J. Chen, K. Raj, et al. 2023. "A Universal Strategy to Promote Secretion of G+/G- bacterial Extracellular Vesicles and Its Application in Host Innate Immune Responses." *ACS Synthetic Biology* 12, no. 1: 319–328.
- Lobritz, M. A., I. W. Andrews, D. Braff, et al. 2022. "Increased Energy Demand From Anabolic-Catabolic Processes Drives β -Lactam Antibiotic Lethality." *Cell Chemical Biology* 29, no. 2: 276–286.
- McMillan, H. M., and M. J. Kuehn. 2021. "The Extracellular Vesicle Generation Paradox: A Bacterial Point of View." *EMBO Journal* 40, no. 21: e108174.
- Nevermann, J., A. Silva, C. Otero, et al. 2019. "Identification of Genes Involved in Biogenesis of Outer Membrane Vesicles (OMVs) in *Salmonella Enterica* Serovar Typhi." *Frontiers in Microbiology* 10: 104.
- Parsons, J. B., and C. O. Rock. 2013. "Bacterial Lipids: Metabolism and Membrane Homeostasis." *Progress in Lipid Research* 52, no. 3: 249–276.
- Percy, M. G., and A. Gründling. 2014. "Lipoteichoic Acid Synthesis and Function in Gram-Positive Bacteria." *Annual Review of Microbiology* 68, no. 1: 81–100.
- Qiao, L., Y. Rao, K. Zhu, X. Rao, and R. Zhou. 2021. "Engineered Remolding and Application of Bacterial Membrane Vesicles." *Frontiers in Microbiology* 12: 729369.
- Rao, Y., H. Peng, W. Shang, et al. 2022. "A Vancomycin Resistance-Associated WalK(S221P) Mutation Attenuates the Virulence of Vancomycin-Intermediate *Staphylococcus aureus*." *Journal of Advanced Research* 40: 167–178.
- Schwechheimer, C., and M. J. Kuehn. 2015. "Outer-Membrane Vesicles From Gram-Negative Bacteria: Biogenesis and Functions." *Nature Reviews Microbiology* 13, no. 10: 605–619.
- Sohlenkamp, C., O. Geiger, and F. Narberhaus. 2016. "Bacterial Membrane Lipids: Diversity in Structures and Pathways." *FEMS Microbiology Reviews* 40, no. 1: 133–159.
- Suri, K., A. D'Souza, D. Huang, A. Bhavsar, and M. Amiji. 2023. "Bacterial Extracellular Vesicle Applications in Cancer Immunotherapy." *Bioactive Materials* 22: 551–566.
- Toyofuku, M., G. Cárcamo-Oyarce, T. Yamamoto, et al. 2017. "Prophage-Triggered Membrane Vesicle Formation Through Peptidoglycan Damage in *Bacillus Subtilis*." *Nature Communications* 8, no. 1: 481.
- Toyofuku, M., N. Nomura, and L. Eberl. 2018. "Types and Origins of Bacterial Membrane Vesicles." *Nature Reviews Microbiology* 17, no. 1: 13–24.
- Toyofuku, M., S. Schild, M. Kaparakis-Liaskos, and L. Eberl. 2023. "Composition and Functions of Bacterial Membrane Vesicles." *Nature Reviews Microbiology* 21, no. 7: 415–430.
- Wang, X., C. D. Thompson, C. Weidenmaier, and J. C. Lee. 2018. "Release of *Staphylococcus aureus* Extracellular Vesicles and Their Application as a Vaccine Platform." *Nature Communications* 9, no. 1: 1379.
- Wang, Y., X. Huang, Z. Hu, et al. 2025. "Oxacillin Promotes Membrane Vesicle Secretion in *Staphylococcus aureus* via a SarA-Sle1 Regulatory Cascade." *Nanoscale* 17, no. 5: 2488–2497.
- Wang, Y., M. Wang, Y. Liu, et al. 2022. "Integrated Regulation of Stress Responses, Autophagy and Survival by Altered Intracellular Iron Stores." *Redox Biology* 55: 102407.
- Yamasaki-Yashiki, S., T. Shiraishi, M. Gyobu, et al. 2024. "Immunostimulatory Activity of Lipoteichoic Acid With Three Fatty Acid Residues Derived From *Limosilactobacillus Antri* JCM 15950^T." *Applied and Environmental Microbiology* 90, no. 10: e0119724.
- Yang, Y., H. Wang, H. Y. Zhou, et al. 2020. "Protective Effect of the Golden Staphyloxanthin Biosynthesis Pathway on Under Cold Atmospheric Plasma Treatment." *Applied and Environmental Microbiology* 86, no. 3: e01998–02019.
- Ye, C., W. Li, Y. Yang, et al. 2021. "Inappropriate Use of Antibiotics Exacerbates Inflammation Through OMV-Induced Pyroptosis in MDR *Klebsiella pneumoniae* Infection." *Cell Reports* 36, no. 12: 109750.
- Yuan, J., J. Yang, Z. Hu, et al. 2018. "Safe Staphylococcal Platform for the Development of Multivalent Nanoscale Vesicles Against Viral Infections." *Nano Letters* 18, no. 2: 725–733.

Supporting Information

Additional supporting information can be found online in the Supporting Information section.